HiSST: 2nd International Conference on
High-Speed Vehicle Science Technology
11–15 September 2022, Bruges, Belgium

Structure Design of a Sounding Rocket Fairing with a Segmented Filament Winding-Ceramic Matrix Composite Thermal Protection System

Giuseppe D. Di Martino[1], Thomas Reimer[2], Lucas Dauth[3], Luis Baier[4]

Abstract

Sounding rocket flight experiments are of fundamental importance for the development and optimization of future space transportation systems. In this framework, the STORT project is focused on the key technologies for the flight at high Mach numbers (higher than 8) for a relatively long time, representative of the operating conditions of high-energetic re-entry flights for reusable first or upper stages. In particular the forebody of the flight experiment carrier, which is subjected to the highest heat loads during the mission trajectory, requires the use of a suitable ceramic matrix composite structure. The present paper describes the activities carried out for the design, validation and construction of the forebody thermal protection system, which is constituted by an inhouse-built C/C-SiC composite structure, made of a bulk conical nose element and four shell segments manufactured via wet filament winding of the carbon fibre with a phenolic resin and subsequent pyrolysis and liquid silicon infiltration.

Keywords: *Ceramic Matrix Composites, Thermal Protection System, Hypersonic Flight Experiment*

1. Introduction

Representative flight experiments play a key role for the development and optimization of future space transportation systems. In fact, on one side they allow to characterize real flight operating conditions compensating the deficits of ground experimental testing. On the other side they are required for collecting valuable data for the validation of numerical analyses.

In the last years the German Aerospace Centre (DLR) has taken part in several projects for the design and construction of sounding rockets and the operation of flight experiments with the objective of demonstrating technologies for reusable first stage launchers. In some of the previous flight experiments [1, 2, 3] hypersonic conditions with Mach numbers up to 10 were reached but for a duration shorter than 30 seconds, limiting therefore the overall aerothermal loads. Other upcoming programs [4, 5] focus on technologies for aerodynamic active control, propellant management, approach and landing in subsonic up to supersonic flight with nominal Mach numbers up to maximum 5. Among them, the project STORT (Key Technologies for High-Speed Return Flights of Launcher Stages) is focused on the key technologies and the thermomechanical challenges encountered by highly thermally stressed components at high Mach numbers (higher than 8) for a relatively long time, of approximately 110 seconds. This allows to increase the integral thermal load obtaining conditions representative of high-energetic re-entry flights in particular for application in reusable first or even upper stages [6].

[1] *DLR Institute of Structures and Design, Pfaffenwaldring 38-40, 70569 Stuttgart, Germany, Giuseppe.DiMartino@dlr.de*
[2] *DLR Institute of Structures and Design, Pfaffenwaldring 38-40, 70569 Stuttgart, Germany, Thomas.Reimer@dlr.de*
[3] *DLR Institute of Structures and Design, Pfaffenwaldring 38-40, 70569 Stuttgart, Germany, Lucas.Dauth@dlr.de*
[4] *DLR Institute of Structures and Design, Pfaffenwaldring 38-40, 70569 Stuttgart, Germany, Luis.Baier@dlr.de*

In the framework of the STORT project the DLR Institute of Structures and Design is responsible for the design and manufacturing of the structure for the forebody of the sounding rocket, which in the mentioned severe flight conditions becomes of extreme importance. In fact, the fluid-dynamic phenomena involved in hypersonic flow include intense shock waves forming in front of the nose tip and of the vehicle leading edges, in which the kinetic energy is dissipated into internal energy in an extremely short distance generating an air plasma state characterized by high temperatures and dissociated and ionized particles [7]. For relatively long exposition times, as in the case of STORT, this requires the design of a suitable thermal protection system (TPS) with use of high-temperature resistant ceramic matrix composite (CMC) materials.

In the present case, the high-temperature shield is a C/C-SiC composite structure, made of a bulk conical nose element and four shell segments with the objectives of minimizing the segmentation of the structure and obtaining an axisymmetric smooth aerodynamic surface. This could be obtained by manufacturing the parts via filament winding of the carbon fibre with a phenolic resin and subsequent pyrolysis and liquid silicon infiltration (LSI).

An overview of the design process, including the numerical analyses for the thermo-mechanical validation of the structure, and of the different steps of the manufacturing of the CMC components is presented in the following.

2. STORT Project

The STORT project is a three-year DLR research project carried out within the framework of the centre's "Reusable Space Transport Systems" program.

As mentioned, the main goal of the project is to develop and test selected technologies related to the thermomechanical analysis and evaluation of launch systems in hypersonic flight conditions for a duration of around 110 seconds. In order to achieve these flight conditions a three-stage sounding rocket configuration has been implemented, with the third stage flying a "suppressed" trajectory at Mach numbers above 8 in a nominal altitude range between 40 and 50 km. The nominal trajectory of the STORT rocket in terms of altitude and velocity is shown in Fig. 1.

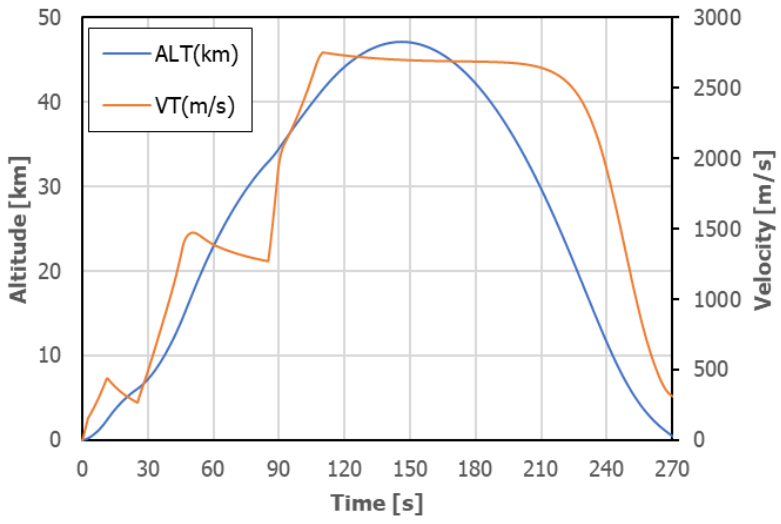

Fig. 1. STORT sounding rocket nominal trajectory [8]

Fig. 2 shows the configuration of the third stage with the scientific payloads.

These include first of all the CMC forebody structure that works as TPS of the vehicle. Moreover, the forebody is extensively instrumented with heat flux sensors, thermocouples and pressure sensors along four longitudinal lines every 90° in circumferential direction in order to get precious data about the vehicle aerothermodynamic and the structure thermal response.

The other experiments, which are described more in detail in [8] and following dedicated articles, include three fixed canards with a CMC outer shell that are used to qualify active and passive thermal

management concepts and a to perform a shock wave-boundary layer interaction experiment; two additional video cameras to monitor the fins of the third stage; a lightweight pure CFRP module for flight qualification; instrumented tailcan and upper stage fins to collect deformation, temperature and pressure data.

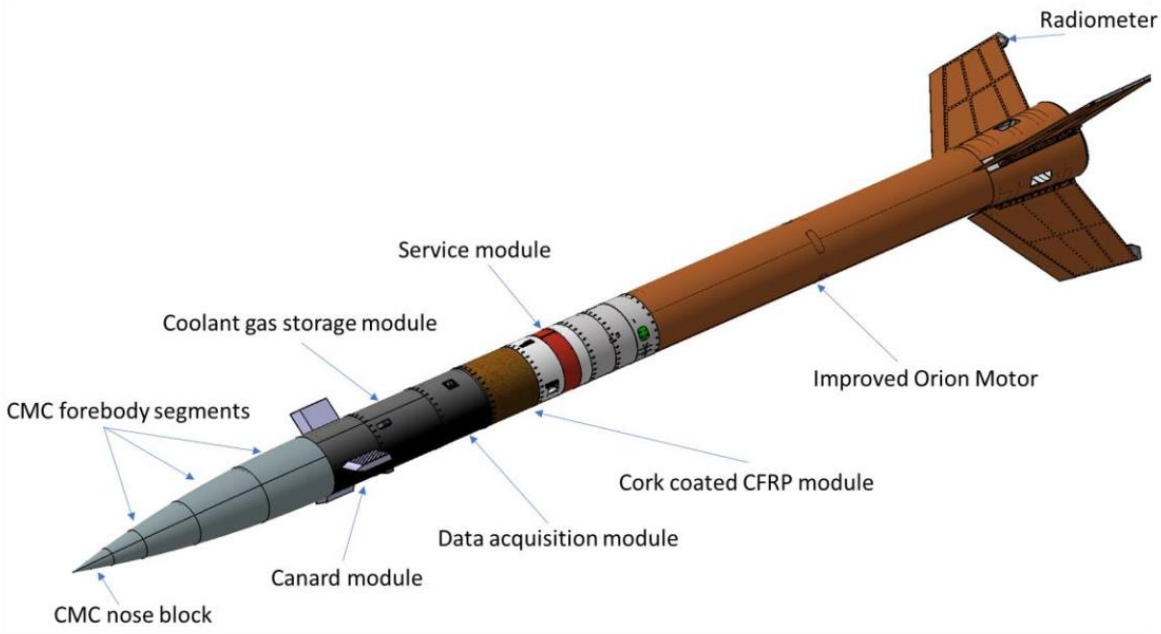

Fig. 2. Third stage of the STORT flight configuration with scientific payloads [8]

The STORT three-stage sounding rocket was successfully launched in the early morning of 26th June 2022 from the Andøya Space launch site in northern Norway. An overview of the main achievements of the flights is given in [8]

3. Design overview

3.1. Structure concept

Fig. 3 shows a section view of the overall design of the rocket forebody with its ceramic TPS, whose length was defined to be 1.5 m.

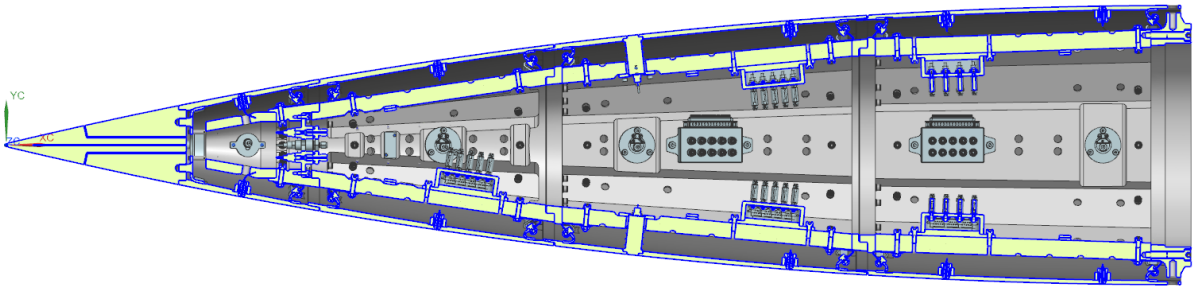

Fig. 3. Section view of the STORT forebody design

One of the main challenges for the TPS construction in the STORT project was to reduce the segmentation as much as possible and obtain an axisymmetric external surface avoiding geometrical edges and discontinuities which typically determine a localized increase of the heat fluxes, as experienced in the previous SHEFEX II program [9]. For this purpose, except for the bulk nose in the most forward position, the TPS was manufactured via filament winding of the carbon fibres. In this way it was possible to divide the full TPS in only five components: as mentioned, a first bulk conical nose with a rounded tip with a radius of 2.5 mm and four axisymmetric shell segments forming the prescribed

aerodynamic shape up to the rocket third stage diameter. In order to prevent that due to the thermal expansion the segments press on each other eventually generating critical internal stress, suitable gaps between the shells are included and filled with a soft graphite-based paste resistant to relatively high temperatures for preserving the aerodynamic shape. The gaps, in particular, were defined on the basis of the thermo-mechanical simulation presented in the following, and are in the order of 1-1.5 mm.

The described CMC components surround an aluminium structure for supporting the sensors integration, attaching electronic components and routing electric cables and for connecting the whole forebody to the rest of the third stage. For the sake of the structure assembly strategy, the metallic understructure is also split in four different main segments, each of which consists of four main longitudinal stringers connecting the forward and backward interface rings. Aluminium sheets with a 2.5 mm thickness close the space between the stringers.

Polycrystalline wool (ALTRA® MAT) is used between the CMC shells and the understructure for providing further thermal insulation.

Following the general concept of a clean external aerodynamic surface, the connection between the CMC parts and the metallic structure was also the subject of a dedicated design, as it will be described in Sec. 3.3.

3.2. TPS thermal analysis

A numerical analysis of the forebody was performed with a simplified approach to have a relatively fast estimation of the structure thermal response during the flight.

In particular, the ANSYS Mechanical software was used to solve the transient energy equation with the Finite Element (FE) technique, considering in the calculation the TPS components and the polycrystalline thermal insulation.

The assigned boundary conditions include:

- a convective heat flux on the TPS external surface;
- a radiative heat flux from the TPS external surface to the ambient considering for the CMC material an emissivity of 0.85;
- thermal contact condition between the TPS and the polycrystalline thermal insulation;
- adiabatic condition on the other surfaces.

For what concerns the estimation of the convective heat flux $\dot{q}_c$ during the flight trajectory the classical equation applies

$$\dot{q}_c = h(T_r - T_w) \tag{1}$$

where h is the heat transfer coefficient, T_r the recovery boundary-layer temperature and T_w the wall temperature.

For the sake of simplicity, in the estimation of the convective heat flux, the TPS external surface was split in six parts: the stagnation region, i.e. the half spherical surface at the nose tip, the remaining conical surface of the bulk nose and the surfaces of each shell segment. For each of them constant conditions are assumed. In particular, when supersonic flight is reached, the asymptotic conditions for each segment are assumed to be the conditions downstream the shock waves forming in correspondence of the trajectory conditions at each instant shown in Fig. 1.

With this assumption, literature correlation formula [10] can be applied for estimating the heat transfer coefficient. For the stagnation region the following equation valid in the hypothesis of laminar flow at the stagnation point of a spherical blunt body with radius R was considered

$$h = 0.763\, Pr_\infty^{-0.6} \sqrt{\frac{V_\infty}{R}\, \rho_\infty \mu_\infty\, f(M_\infty, \gamma)\, c_p} \tag{2}$$

For the remaining surfaces of the TPS the heat flux coefficient was estimated as

$$h = St \;\; c_p \, \rho_\infty \, V_\infty \tag{3}$$

and the correlation formula for a laminar flow along a flat plate of characteristic length L, with the Mangler transformation for axisymmetric bodies [11], is considered for calculating the Stanton number as

$$St = \sqrt{3} \times 0.664 \, Pr^{-\frac{2}{3}} \, Re_L^{-\frac{1}{2}} \tag{4}$$

The recovery boundary-layer temperature on the other hand is calculated as

$$T_r = T_\infty \left(1 + \sqrt{Pr_\infty} \frac{\gamma - 1}{2} M_\infty^2\right) \tag{5}$$

Finally, the wall temperature is also initially unknown. For this reason, the following iterative procedure is needed. A first trial convective heat flux is calculated with Eqs. (1) to (5) in cold wall condition, i.e for $T_w = 300$ K. The transient thermal simulation is performed in ANSYS with the trial convective heat flux as boundary condition. From the results of the thermal simulation the time profiles of the wall temperature averaged on each surface is obtained, which then allows to calculate a new trial convective heat flux. This procedure is then iterated until the maximum relative error of the wall temperature between one step and the previous one is smaller than 5%.

Fig. 4 shows the converged results in terms of the time profiles of the convective heat flux and of the maximum wall temperature for each segment, while Fig. 5 shows the calculated temperature distribution on the TPS at t=230 s, i.e. around the time when the maximum values of the temperature are reached for all segments. From these results it can be noticed that the heat flux is significantly high especially in the stagnation region, which consequently reaches very high temperatures. In particular, the nose tip reaches a temperature of 1900 K around t=180 s, after which active oxidation of the C/C-SiC material can be expected, depending on environmental pressure. Likely, this behavior would lead to a material loss and a consequent increase of the tip radius, which in turn will reduce the convective heat flux according to Eq. (2). However, looking at the time profile of the maximum temperature and at the temperature distribution in the TPS, it can be concluded that the material active oxidation is expected to happen for a relatively short time, affecting a very small region of the nose, where the temperature quickly decreases, while the shell segments stay well below the transition temperature, reaching maximum temperatures in the range 1200-1500 K.

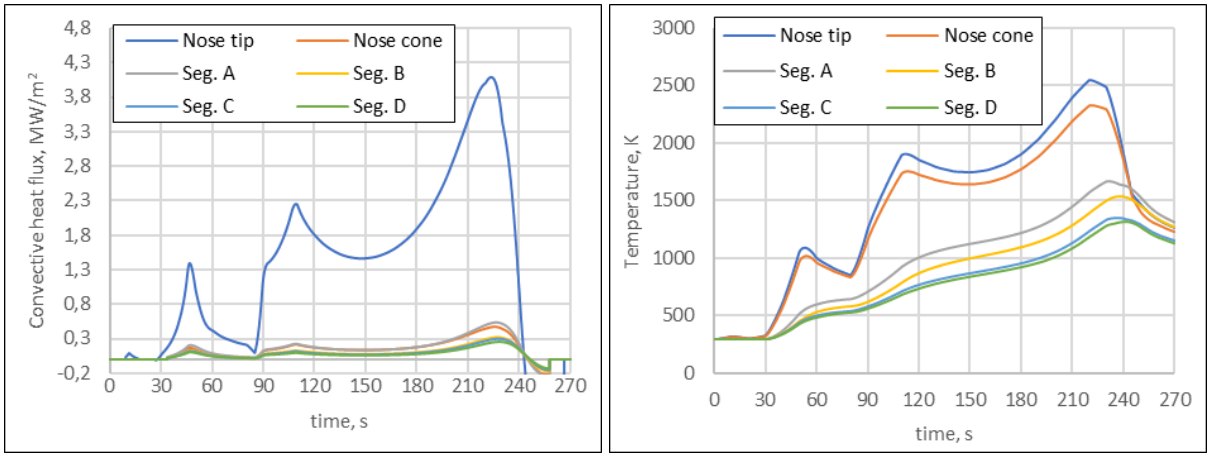

Fig. 4. Time profile of the convective heat flux and the corresponding maximum temperature for each TPS segment

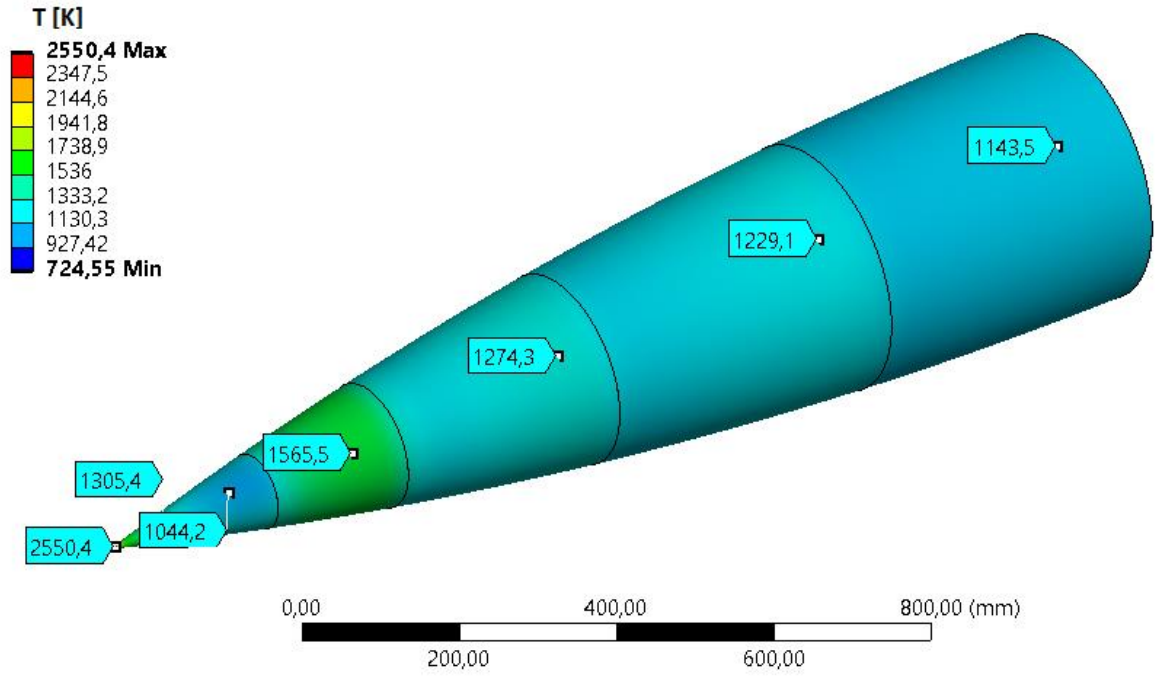

Fig. 5. Calculated temperature contour on the TPS at t=230 s

Other important information for the structure design that could be obtained from the described thermal simulation include, for example, the temperature on the back of the nose cone, where stainless steel tubes for flow pressure measurements are integrated, which reaches a maximum temperature around 720 K, and the temperature on the inner surface of the polycrystalline insulation, which stays for the largest part below 350 K, increasing only in the region of segment A up to values around 650 K.

Moreover, the TPS temperature distribution constitutes an important load case for the thermo-mechanical validation of the forebody structure, in particular for what concerns the connection between the ceramic shells and the metallic understructure, as it will be shown in the next sections.

3.3. Connection elements between TPS and understructure

The definition of a suitable concept for the connection of the TPS to the metallic understructure, which assures the needed mechanical resistance under different types of loads, providing at the same time a good resistance to the strong temperature gradient from the high temperature experienced on the TPS to the near-ambient temperature of the metallic, is of fundamental importance in the design process.

In the case of STORT the task was made even more challenging by the axisymmetric geometry of the CMC segments and by the requirement of keeping the external aerodynamic shape unaffected. The latter implies that no bolted connection or rivets could be used on the TPS. For this reason, the application of the so called in-situ joining technique was the selected technological choice.

In particular, the in-situ joining is an inhouse-developed technique for producing thicker and geometrically complex C/C-SiC components produced via LSI [12] from inidvidual simple pieces. It consists of fixing together two different components when they are still in the porous C/C status (i.e. after pyrolysis and before siliconization) using a carbonaceous paste to enrich the gaps of the parts. During the silicon infiltration, the low amount of paste pyrolyzes, while the capillary effect combined with the low viscosity of the molten silicon ensures a quick filling of the composite and the joint area.

The described process implies that the connection elements should be also made from the same CMC material, becoming during the siliconization process an integral part of the TPS main components.

In the present project, three different configurations have been taken into consideration, which are shown in Fig. 6 for the example case of segment B. A comparative study between them was carried out based on four main issues: the connection elements manufacturing, the joining process to the shells, the coupling with the understructure and the mechanical resistance.

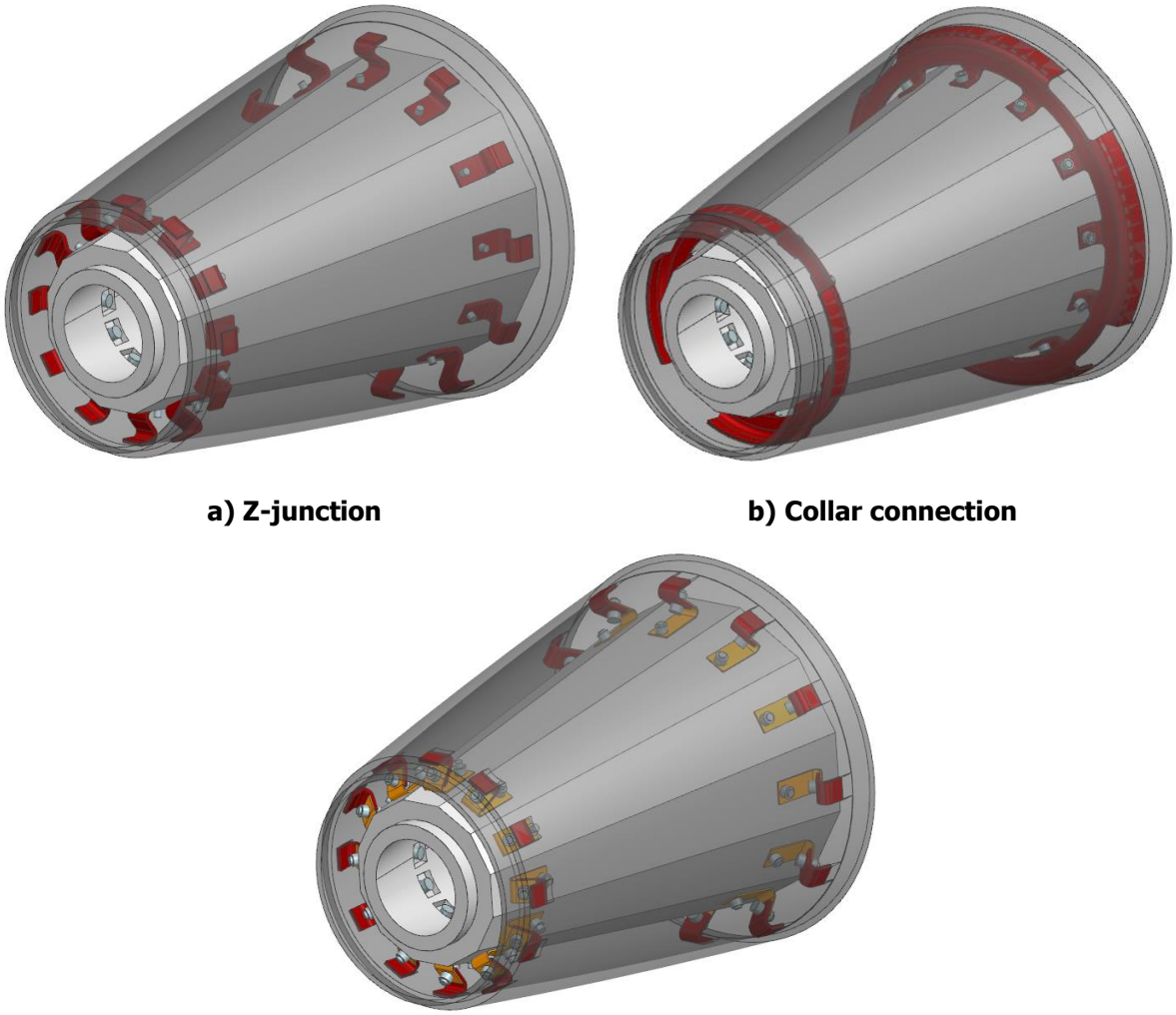

a) Z-junction **b) Collar connection**

c) Two-L connection

Fig. 6. Concepts for the connection between TPS shell and understructure

The first configuration foresees the application of CMC z-shaped junction elements, following a concept similar to the one employed in SHEFEX II (with the difference that in that case the connection elements were riveted to the TPS panels via ceramic screws) [2]. This configuration has the advantage that the element geometry is the same everywhere and the manufacturing is easy and efficient. Moreover, the geometrical shape allows a good control over the mechanical stresses, especially in view of the thermal expansion of the shells. On the other side, the joining process of the junctions to the ceramic segment poses the issue of the reliability, since the joining surface is relatively small and the process has to be applied several times. Finally, it has to be taken into consideration that the tolerance intrinsic in the joining process could give problem in the coupling with the understructure.

In order to solve the mentioned drawbacks of the configuration with the z-elements, the second consideration with collar connections was considered. In fact, in this case only two joining processes per segment have to be applied and the joining surface is considerably larger. This would make also the final component more stable, allowing for machining at the interfaces with the understructure for compensating eventual misalignments. On the other side, since in this case the geometry of the component is more complex and different for each section, the manufacturing process is more expensive. Finally, as it will be shown in the next section, in this case the overall connection has a higher stiffness, which results in higher stresses in the material.

The last configuration is a variant of the first one in which the connection elements are split in two parts: the first half made of CMC to be joined to the TPS and the second half made of a 0.8 mm-thick Inconel for the interface to the understructure, the two parts being connected with Inconel bolts. In this case the manufacturing of the two pieces is still very easy and efficient, although the issue of the

reliability of the joining process is also similar to what was discussed for the first configuration. On the other side the last configuration gives two important advantages. First, suitable tolerances in the hole for the bolted connection between the two pieces can compensate for eventual alignment errors due to the joining. Furthermore, the addition of a thin metallic bracket allows to relieve the mechanical stresses in the ceramic element.

The discussed considerations are summarized for convenience in Table 1.

Table 1. Trade-off between different configurations for the connection between TPS and understructure

	Z-junctions	**Collar connections**	**Two-L connections**
Manufacturing	Easy and efficient	Different dimension in each section Additional cost	Easy and efficient
Joining	Small joining surface N joining per section	Larger joining surface Joining in one step for each section	Small joining surface N joining per section
Coupling with understructure	Subject to misalignments Small resistance for post machining	Higher stability and resistance for machining after joining	Misalignments correction via the metallic element
Mechanical stress	Good control over stresses	Higher stiffness → Higher stresses	Best control over stresses

Based on the discussion presented above, the "Two-L connections" configuration was chosen for the forebody of STORT.

3.3.1. Connection of the nose and segment A

A dedicated discussion is needed for the configuration designed for the connection of segment A and the nose cone, which is shown in Fig. 7.

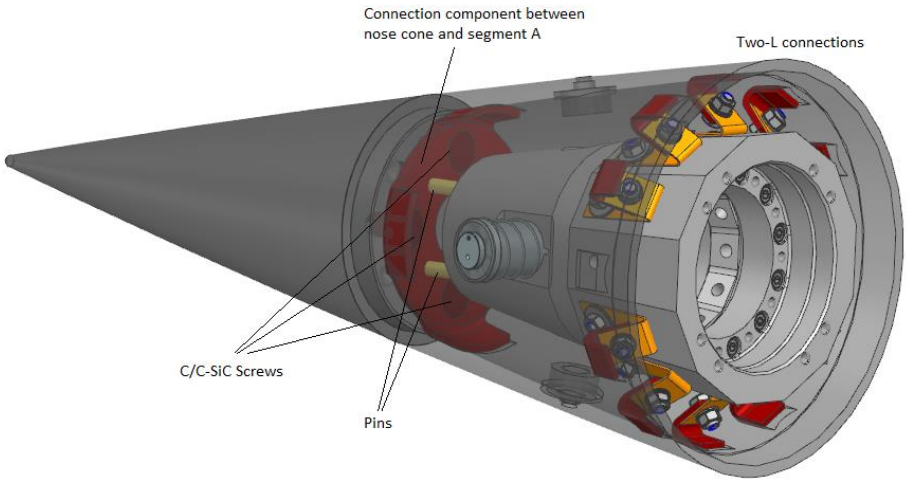

Fig. 7. Nose cone and segment A design

In fact, in this case the two-L connection configuration chosen for the other segments could be applied to connect the TPS to the understructure only on the rear part. Moreover, in this case, to allow the sensor integration, only 10 instead of 12 junctions are implemented.

On the forward part the connection between the nose cone and the shell component is realized. For this an additional disc component is included, also made of C/C-SiC, which is joined to the internal surface of the shell and presents 4 holes through which 4 ceramic screws ensure the connection to threaded holes eroded in the tip. 4 dowel pins bolted on the front face of the understructure and passing through the CMC disc constrain the relative rotational motion between the TPS group and the understructure avoiding the whole corresponding bending load from the tip loads to be transferred only by the two-L connections.

3.4. Thermo-mechanical structure validation

The ANSYS Mechanical software was employed to carry out static mechanical simulation of the forebody with the FE method in order to support the design process and validate the overall resistance of the structure.

Assuming that the interaction between two following TPS components is negligible, each segment was analyzed separately. For each of them, the TPS shell, the connection elements, the polycrystalline thermal insulation and the aluminum understructure were included in the model. A fixed boundary constraint was set on the back interface of the understructure. A bonded contact was set between the ceramic connection elements and the TPS, while the bolted connections were modeled in detail with frictional contacts between the parts and pretension of the bolt.

Different load conditions were simulated representative of the critical loads expected during the flight trajectory.

3.4.1. Thermal load

The first load condition is represented by the temperature distribution calculated with the analysis described in Sec. 3.2, which leads to the thermal expansion of the CMC component, while the aluminum structure remains cold and consequently undeformed.

This load condition was considered also for analyzing the different configurations, considering the case of Segment B described in Sec. 3.3 and supported the last row of Table 1. Fig. 8 shows the results in terms of the maximum principal stress distribution in the connection element at t=230 s.

It can be observed that, as discussed previously, the collar connection is too stiff and the thermal expansion of the external shell would lead to very high stresses, way above the limit of the C/C-SiC material, whose bending maximum stress is around 180 MPa.

The z-shaped connections provide a better behavior with acceptable stresses for the same thermal load condition.

But it is especially with the two-L configuration that the CMC element has significantly lower stress, which is absorbed in great part from the Inconel bracket, which is subjected to stresses up to 290 MPa, which are anyway low compared to the material maximum stress (for the Inconel 600 the maximum stress is in the range 550-690 MPa).

As mentioned, the two-L connection configuration was chosen. Consequently, this configuration was validated with respect to the thermal load conditions for all segments. The main results are summarized in Table 2.

Table 2. Main results of the static mechanical simulation in the case of thermal load

	Segment A	Segment B	Segment C	Segment D
Maximum axial displacement, mm	0.71	0.62	0.88	0.69
Maximum radial displacement, mm	0.64	0.56	0.71	0.62
Max. stress in CMC element, MPa	158.0	89.9	117.9	96.4
Av. shear stress at the joint surface, MPa	2.91	0.73	0.76	1.55

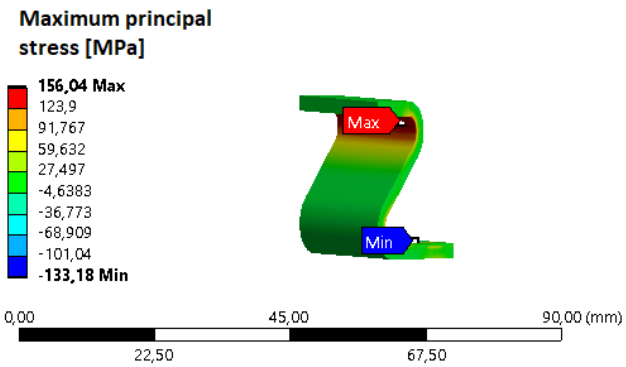

a) Z connection

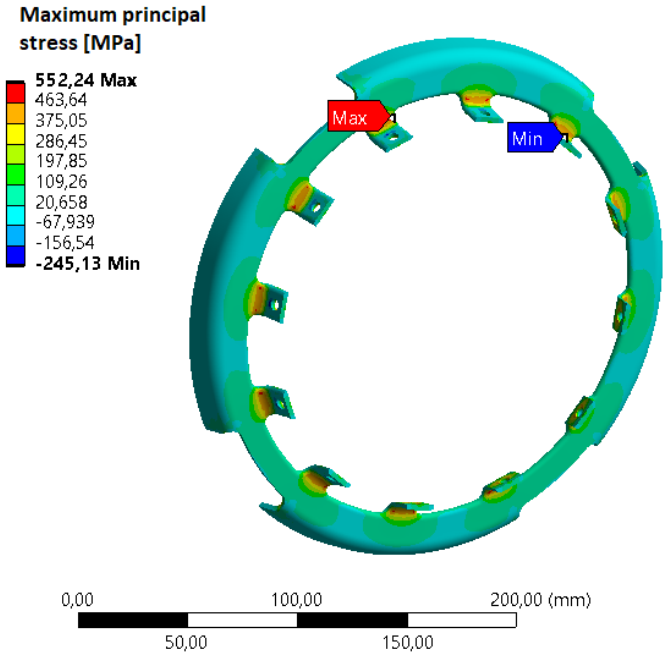

b) Collar connection

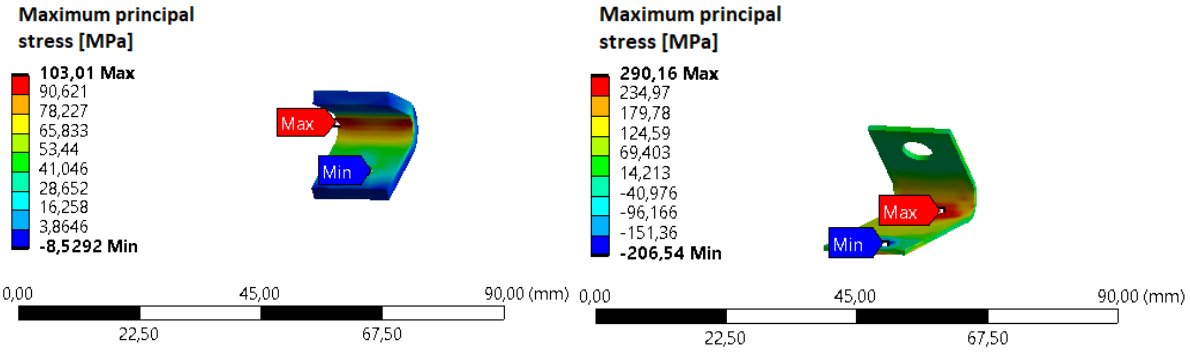

c1) Two-L connection – CMC **c2) Two-L connection – Inconel**

Fig. 8. Maximum principal stress distributions in the different connection configurations for the case of pure thermal load at t = 230 s

3.4.2. Combined thermal and aerodynamic pressure load

The aerodynamic simulation of the STORT payload was carried out by the DLR Institute of Aerodynamics and Flow Technology (AS-HYP) to determine the aerodynamic load to which the structure is subjected in different points of the trajectory for different possible angles of attack. The most critical condition in terms of pressure load was determined to be at t=217.9 s at an angle of attack of 10°. The corresponding pressure distribution is shown in Fig. 9.

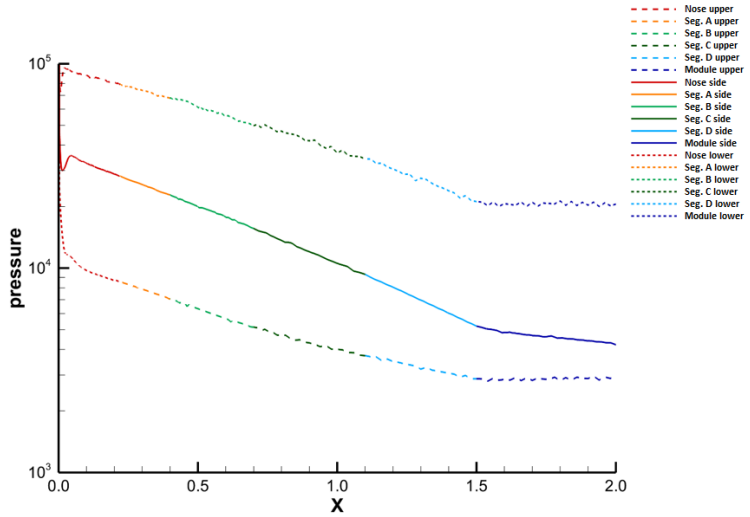

Fig. 9. Pressure distribution along the forebody at t=217.9 s at an angle of attack of 10°

The presented pressure load, interpolated on the surface of each segment, was considered in combination with the temperature distribution calculated at the same time t=217.9 s as second load condition for the validation of the structural resistance. The corresponding deformation is shown in Fig. 10 for the example case of segment B (the thermal isolation is hidden from the figure to show the behavior of the connection elements). It can be noticed that in this case the load is not axisymmetric and the connection elements are partly pressed and partly pulled. The main results for the different segments are reported in Table 3.

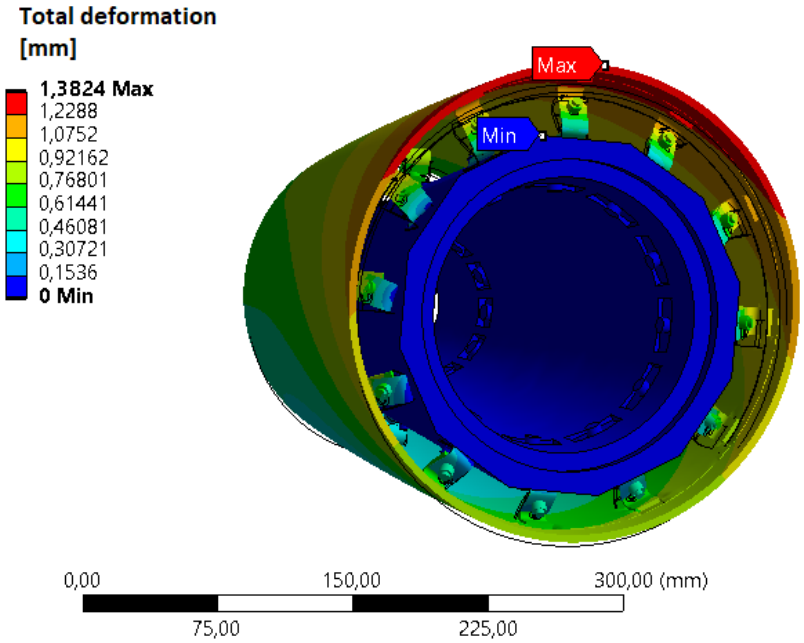

Fig. 10. Total deformation of segment B under combined aerodynamic pressure and temperature load

Table 3. Main results of the static mechanical simulation in the case of the critical aerodynamic pressure and thermal load at t=217.9 s

	Segment A	Segment B	Segment C	Segment D
Maximum axial displacement, mm	0.78	0.77	1.08	0.75
Maximum radial displacement, mm	0.57	1.25	1.68	0.96
Max. stress in CMC element, MPa	148.5	131.6	155.3	170.7
Av. shear stress at the joint surface, MPa	3.09	0.76	0.75	2.73

3.4.3. Acceleration load

The last load condition considered is the acceleration load, important in the first part of the flight. In particular, based on data measured for the SHEFEX II flight a value of 40 g was fixed and applied once in the axial direction and once in the transversal direction. The main results are summarized in Table 4 and Table 5 respectively.

Table 4. Main results of the static mechanical simulation in the case of the axial acceleration load

	Segment A	Segment B	Segment C	Segment D
Maximum axial displacement, mm	0.14	0.16	0.29	0.36
Maximum radial displacement, mm	0	0	0	0
Max. stress in CMC element, MPa	47.4	52.1	43.8	54.3
Max. shear stress at the joint surface, MPa	0.24	0.14	0.23	0.59

Table 5. Main results of the static mechanical simulation in the case of the transversal acceleration load

	Segment A	Segment B	Segment C	Segment D
Maximum axial displacement, mm	0.09	0.09	0.03	0.02
Maximum radial displacement, mm	0.31	0.25	0.40	0.41
Max. stress in CMC element, MPa	44.1	51.6	78.5	84.4
Max. shear stress at the joint surface, MPa	0.20	0.17	0.27	1.15

4. CMC structure manufacturing and assembly

For the sake of completeness, the different steps of the manufacturing of the C/C-SiC TPS structure are listed and shown in pictures in the following. The detailed description will be the subject to following works.

The manufacturing of C/C-SiC components involves always the following steps:

- Manufacturing of the initial part made of carbon fiber reinforced polymer (CFRP)
- Pyrolysis process through which the matrix is carbonized and the part passes to the C/C status
- Eventually, in-situ joining of different parts in C/C-state for obtaining complex geometries and/or thicker components
- Liquid silicon infiltration to create the C/C-SiC final component

For the nose cone, in particular, three 30 mm-thickness plates were produced via the Hot Pressing method and pyrolyzed to the C/C status. Then they were joined together, siliconized and finally machined to obtain the final component, which is shown in Fig. 11.

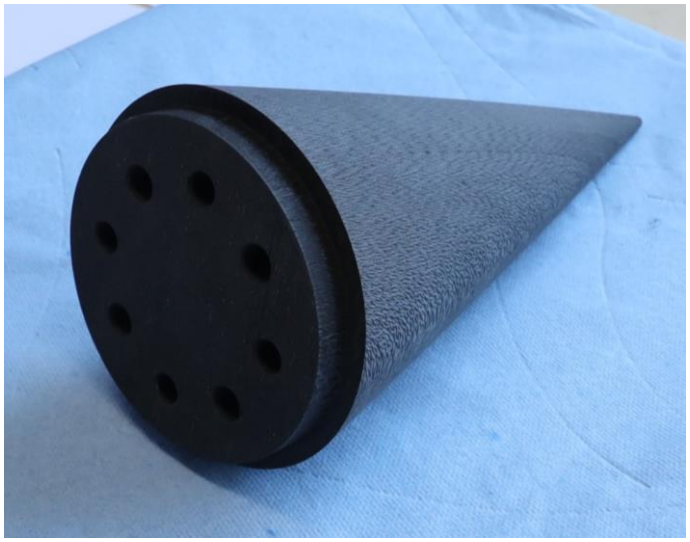

Fig. 11. STORT rocket nose cone

For the shell segments, as already mentioned, the wet filament winding technology was chosen for the fabrication of the initial CFRP parts. A picture of the ongoing process with the winding of the pre-impregnated fibres around a dedicated mandrel for the example case of segment B is shown in Fig. 12.

Fig. 12. Manufacturing of the TPS segment B in the CFRP initial status via filament winding.

Fig. 13 shows then the same segment B just after the pyrolysis process, i.e. in C/C-status, before and the machining to the final geometry. In the present work, it was preferred to perform the machining to the final geometry in the C/C-status, because in this way the material is still not too hard giving the possibility to do the machining a lot faster.

a) Before machining **b) After machining**

Fig. 13. Segment B in C/C-status

In parallel, also the ceramic part of the connection elements was manufactured again with the hot pressing technology, utilizing suitably designed molds, obtaining after the pyrolysis and the machining the components in C/C-status shown in Fig. 14.

Fig. 14. Connection elements in C/C state.

At this point the joining of the connection to the main shell components could be performed. Also in this case dedicated tools were designed and manufactured to allow the application of the needed pressure on the joining area and the correct relative alignment of the parts in the process, as shown in Fig. 15a. Fig. 15b shows, again in the case of segment B, the final component with all connection elements joined in the C/C-status.

The end component after the siliconization is then shown in Fig. 16.

Finally, the STORT forebody fully assembled is shown in Fig. 17, while Fig. 18 shows the forebody integrated on the fully assembled STORT rocket on the launch rail ready for the flight.

a) Joining process **b) Segment B after the joining of all connection elements**

Fig. 15. Joining of the connection elements to the main shell

Fig. 16. Segment B in C/C-SiC final status

5. Conclusions

In the framework of the DLR's "Reusable Space Transport Systems" program, the STORT project main objective was the design, integration and operation of a three-stage sounding rocket for testing key technologies at hypersonic Mach numbers, higher than 8, for a relatively long time, of approximately 110 seconds. In order to protect the rocket from the very high thermal load to which the external surface is subjected in these operating conditions, especially at the tip, the DLR Institute of Structure and Design was responsible for the design, validation and manufacturing of the forebody TPS made of inhouse-built C/C-SiC components.

In the present paper, the design process has been presented, starting from the general concept, based mainly on the application of CMC axisymmetric shell segments, manufactured via filament winding of the carbon fibres, in order to reduce geometrical discontinuities and sharp edges, where typically the heat loads increase. The different considered configurations were described and after a detailed trade-off of the advantages and disadvantages the so-denominated "Two-L connection" configuration was selected. This consists of 12 junctions for each section, which are made of a first C/C-SiC bracket joined to the main TPS shell and a thin Inconel bracket for the coupling to the understructure.

Fig. 17. STORT forebody fully assembled

Fig. 18. STORT rocket fully assembled on the launch rail

Numerical analyses were then carried out to have a fast estimation of the material thermal response during the flight and to validate the structural resistance under different critical load conditions.

Finally, a general overview of the manufacturing steps for the C/C-SiC components is shown.

References

1. Weihs, H., Longo, J., Gülhan, A.: Sharp Edge Flight Experiment SHEFEX. Fourth European Workshop on Thermal Protection Systems and Hot Structures Conference Proceedings, ESA SP-521 (2002).
2. Weihs, H., Longo, J., Turner, J.: The Sharp Edge Flight Experiment SHEFEX II, a Mission Overview and Status. 15th AIAA International Space Planes and Hypersonic Systems and Technologies Conference, AIAA 2008-2542 (2008). https://doi.org/10.2514/6.2008-2542
3. Gülhan, A., Siebe, F., Klingenberg, F., Kallenbach, A., Petkov, I.: Main Achievements of the Sounding Rocket Flight Experiment ATEK. 72nd International Astronautical Congress (IAC), IAC-21,D2-6.4,x62713 (2021).
4. Bauer, W., et al.: DLR Reusability Flight Experiment ReFEx. Acta Astronaut., 168, 57-68 (2019). https://doi.org/10.1016/j.actaastro.2019.11.034
5. Guédron, S., Ishimoto, S., Dumont, E.: CALLISTO: a Cooperation for an In-Flight Demonstration of Reusability. 70th International Astronautical Congress (IAC), IAC-19,D2,6,1,x52961 (2019).
6. Ecker, T., Karl, S., Dumont, E., Stappert, S., Krause, D.: Numerical Study on the Thermal Loads During a Supersonic Rocket Retropropulsion Maneuver. J. Spacecraft Rockets 57 (1), 131-146 (2019). https://doi.org/10.2514/1.A34486
7. Savino, R., Criscuolo, L., Di Martino, G.D., Mungiguerra, S.: Aero-thermo-chemical characterization of ultra-high-temperature ceramics for aerospace applications. J. Europ. Ceram. Soc. 38 (8), 2937-2953 (2018). https://doi.org/10.1016/j.jeurceramsoc.2017.12.043
8. Gülhan, A., Hargarten, D., Klingenberg, F., Siebe, F., Di Martino, G., Reimer, T.: Main Results of the Hypersonic Flight Experiment STORT. 2nd International Conference on High-Speed Vehicle Science Technology (2022).
9. Gülhan, A., Neeb, D., Thiele, T., Siebe, F.: Aerothermal Postflight Analysis of the Sharp Edge Flight Experiment-II. J. Spacecraft Rockets 53 (1), 153-177 (2016). https://doi.org/10.2514/1.A33275
10. Van Driest, E.R.: The Problem of Aerodynamic Heating. Aeronaut. Eng. Review 15 (10) (1956).
11. Mangler, W.: Boundary Layers at Bodies of Revolution in Symmetric Flow. AVA Report 45/A/17 (1945).
12. Kochendorfer, R., Lutzenburger, N., Weihs, H.: Joining Techniques for Fibre Ceramic Structures. Adv. Composites Letters 13 (1) (2004). https://doi.org/10.1177/096369350401300106